

1 **SO₂ noontime peak phenomenon in the North China Plain**

2 **W. Y. Xu¹, C. S. Zhao^{1,*}, L. Ran², W. L. Lin^{3,4}, P. Yan^{3,4}, X. B. Xu³**

3

4 [1]{Department of Atmospheric and Oceanic Sciences, School of Physics, Peking University,
5 Beijing, China}

6 [2]{Key Laboratory of Middle Atmosphere and Global Environment Observation, Institute of
7 Atmospheric Physics, Chinese Academy of Sciences, Beijing, China}

8 [3]{Key Laboratory for Atmospheric Chemistry, Institute of Atmospheric Composition,
9 Chinese Academy of Meteorological Sciences, Beijing, China}

10 [4]{Meteorological Observation Center, China Meteorological Administration, Beijing, China}

11

12 * Correspondence to: C. S. Zhao (zcs@pku.edu.cn)

13

14 **Abstract**

15 A phenomenon of frequent noontime SO₂ concentration peaks was discovered in a detailed
16 analysis of the SO₂ concentrations in the North China Plain (NCP). The possible causes and
17 their contributions are analysed. The impacts of such a phenomenon on the sulphur cycle were
18 studied and the implications of the phenomenon for atmospheric chemistry, cloud physics and
19 climate were discussed. Different from the more common SO₂ diurnal patterns with high
20 nighttime concentrations, NCP witnessed high frequencies of noontime SO₂ peaks, with an
21 occurrence frequency of 50 to 72% at four stations. Down-mixing of elevated pollution layers,
22 plume transport processes, mountain-valley-winds and fog/high RH haze events were the
23 possible causes. The contribution of each process varies from day to day and from station to
24 station, however, none of those four processes can be neglected. SO₂ peaks occurring during
25 noontime instead of nighttime will lead to a 13 to 35% increase in sulphur dry deposition, 9 to
26 23% increase in gas phase oxidation and 8 to 33% increase in aqueous phase conversions, which
27 will increase the hygroscopicity and the light scattering of aerosols, thus having important
28 impacts on atmospheric chemistry, cloud physics and climate.

29

1 **1 Introduction**

2 High emissions and concentrations of sulphur dioxide (SO₂) have been observed in the North
3 China Plain (NCP) (Lin et al., 2012;Xu et al., 2011b;Zhao et al., 2013), which exerts great
4 impacts on aerosol hygroscopicity and cloud physics (Liu et al., 2011). Yet, the special
5 topography, emission distribution and meteorological conditions in the NCP have complicated
6 the variation of SO₂ concentrations.

7

8 The diurnal variation of primary gas pollutants in polluted regions is typically characterized by
9 morning and evening peaks, due to both the diurnal variations of the planetary boundary layer
10 height (PBLH), emissions and the diurnal variation in photochemistry (Jacobson, 2002). The
11 SO₂ diurnal variation pattern observed in both the Yangtze-River-Delta region (Wang et al.,
12 2002;Qi et al., 2012) and the Pearl-River-Delta region (Wang et al., 2001), as well as that
13 observed in other parts of the world (Khemani et al., 1987;Psiloglou et al., 2013) seem to mostly
14 comply to this rule, with a few exceptions found by Qi et al. (2012).

15

16 The chemical transformation of SO₂ is most rapid during noontime, when the photochemistry
17 is most active and concentrations of oxidants such as the OH radical, H₂O₂ and O₃ are highest
18 (Hua et al., 2008;Ran et al., 2011). OH is the main oxidant for gas phase SO₂ scavenging, while
19 H₂O₂ and O₃ are the major oxidants in aqueous phase SO₂ scavenging processes (Seinfeld and
20 Pandis, 2006). If SO₂ peak values occurred during noontime instead of during nighttime,
21 sulphur conversions would be enhanced, increasing sulphate concentration in aerosols, leading
22 to higher aerosol hygroscopicity and more light scattering.

23

24 Adame et al. (2012) reported rare cases of SO₂ peaking during noontime in Central-Southern
25 Spain, which they attributed to transport from industrial regions. Antony Chen et al. (2001)
26 observed a SO₂ noontime peak only in one out of five measurement periods in Maryland (USA),
27 which were attributed to down-mixing from elevated sources. While this phenomenon seems
28 to be a rare case all over world, several sites in the NCP shows long-term averaged diurnal
29 variation patterns with such variation characteristics (Lin et al., 2011;Lin et al., 2009;Lin et al.,
30 2012;Lin et al., 2008). Short-term observations at both rural and urban sites in the NCP also
31 captured such variation patterns (Gao et al., 2013;Wang et al., 2006b). Long-term
32 measurements at rural sites in the Yangtze River Delta region also displayed pre-noon SO₂
33 peaks that were not in accordance with the diurnal variation pattern of other primary gas

1 pollutants (Ding et al., 2013; Qi et al., 2012), however, observations during shorter campaigns
2 seem to disagree with these results (Wang et al., 2004). Averaged diurnal patterns usually have
3 large standard deviations due to the high seasonal variability of SO₂ and can be significantly
4 influenced by strong pollution episodes. Thus, the representativeness of such averaged profiles
5 and how common such events are is uncertain. Similarly, their cause or the possible impacts
6 such diurnal variation patterns might have is still not clear. The peak occurrence time at the
7 different type of sites differed from each other, the reason behind that still needs to be found.

8
9 In this study, an elaborate investigation into the SO₂ diurnal variation pattern is made based on
10 observations from four stations in the NCP. Possible causes for the noontime peaks and their
11 relative importance are discussed. Finally, the possible impact of such events on the sulphur
12 cycle is investigated and its influence on atmospheric chemistry and climate are pointed out.

13 **2 Data and Methodology**

14 **2.1 Site and Measurements**

15 Measurements of SO₂ and CO (Carbon Monoxide) were carried out at Wuqing meteorological
16 station (WQ, 39°22'58.8"N 117°1'1.2"E, 7.4m a.s.l.) in the NCP during the Haze in China
17 (HaChi) campaign (Jul 2009 to Jan 2010). WQ is located in the heart of the plain region and
18 has been proven to be highly representative of the polluted NCP region (Xu et al., 2011a).

19
20 Measurements from Jan 2009 to Jan 2010 at the Shangdianzi site (SDZ, 40.65°N, 117.12°E,
21 293.9 m a.s.l.), the China Meteorological Administration site (CMA, 39.95°N, 116.32°E,
22 96 m a.s.l.) and the Gucheng site (GCH, 39.13°N, 115.12°E, 15.1 m a.s.l.) made by the Chinese
23 Academy of Meteorological Sciences (Lin et al., 2011; Lin et al., 2009; Lin et al., 2012; Lin et
24 al., 2008) were used as references.

25
26 Radiosonde data from Mar 2009 to Feb 2010 measured at the Nanjiao meteorological station
27 (NJ, 39.8 °N, 116.46°E, 33 m a.s.l.) were used to analyse the temperature inversion within the
28 PBLH to better understand the vertical mixing process. The radiosonde measurements were
29 carried out every day at 8 am. The temperature inversion depth of each day was determined and
30 the occurrence frequencies of different inversion depths were counted for spring (Mar to May

1 2009), summer (Jun to Aug 2009), autumn (Sep to Nov 2009) and winter (Dec 2009 to Feb
2 2010), respectively.

3
4 The locations of the sites as well as the distribution of SO₂ column concentrations retrieved
5 from the Ozone Monitoring Instrument (OMI) on board AURA satellite (OMSO2Readme file,
6 http://so2.gsfc.nasa.gov/Documentation/OMSO2ReleaseDetails_v111_0303.htm) are shown
7 in Figure 1.

8
9 The SO₂ polluted NCP is surrounded in the north by the Yan Mountains and to the west by the
10 Taihang Mountains. The SDZ, CMA and GCH sites are aligned along a northeast – southwest
11 line east to the Taihang Mountains, while WQ is about 80 km to the southeast of the CMA site.
12 The SDZ, CMA, GCH and WQ sites respectively represent the relatively clean background, the
13 polluted urban, rural and suburban area. SO₂ concentrations are high in the south and relatively
14 lower in the north.

15
16 A set of commercial trace gas instruments (Thermo Environmental Instruments Inc., USA C-
17 series) has been used to continuously monitor various trace gases. SO₂ was measured with
18 pulsed UV fluorescence analysers (TE 43CTL) and CO with gas filter correlation analysers (TE
19 48C). Measured gas concentrations were recorded as 1-min average mixing ratios by volume
20 (ppbv), then averaged into 1 hour resolutions. Details on the measurements and data calibration
21 can be found in Lin et al. (2012) and Xu et al. (2011b).

22 **2.2 Determination of SO₂ noon peak phenomenon**

23 Due to the increased emissions, lower boundary layer heights and slower chemical conversions
24 in winter, SO₂ concentrations show significant seasonal variations. In the study of the average
25 SO₂ diurnal pattern, the enhanced signals of wintertime SO₂ data need to be avoided. SO₂ and
26 CO concentrations were divided by the daily maximum value of each day, to acquire the daily
27 normalized diurnal pattern.

28 Afterwards, patterns with peaks only occurring before 9 am or after 4 pm were grouped into the
29 Nighttime-Peak group (group 1), while patterns of peaks only occurring during 9 am to 4 pm
30 were classified into the Noontime-Peak group (group 2). Diurnal patterns with both a noontime
31 and a nighttime peak during the same day were put into the Nighttime & Noontime group (group

1 3). The normalized diurnal variation patterns in each group were averaged and the standard
2 error of the mean ($SEM = \sigma/\sqrt{n}$) was calculated for each hour of day. The occurrence
3 frequency of each group was calculated for each month of 2009 and for the whole measurement
4 period.

5 **2.3 Four possible causes for the SO₂ noon peak phenomenon**

6 Four possible causes for the SO₂ noontime peak phenomenon should be evaluated, the down-
7 mixing for elevated SO₂ pollution layers, the transport of plumes, the influence of mountain-
8 valley breezes and the impact of severe haze or fog events. The diurnal SO₂ profiles of group 2
9 and group 3 were analysed together with the according CO, wind, RH and temperature diurnal
10 profiles to determine which of the above four causes has led to the occurrence of the noon peak.
11 Then the contribution of each cause is yielded by dividing the number of noon peak cases
12 caused by a certain factor with the total number of noon peak cases.

13 If the noon peak was caused by the down-mixing of elevated SO₂ pollution layers, the peak
14 should occur during the early noon time (9 to 12 LT) when the PBL is developing. Thus, cases
15 with SO₂ peaks occurring after the morning peak of CO along with the development of the PBL
16 were filed under the down-mixing case category. The development of the PBL is represented
17 by the increase in surface temperature.

18 CO has a relatively longer lifetime, thus is a very good tracer for pollution plumes. Days with
19 the correlation coefficient between noontime SO₂ and CO reaching a significance level of 95%
20 were categorized into the plume transport case. Averaged correlation coefficients respectively
21 reached 0.81, 0.82, 0.84 and 0.73 in SDZ, CMA, GCH and WQ.

22 Due to the topography of the NCP, all four sites are under the influence of mountain valley
23 circulations, especially the SDZ, CMA and GCH sites. Winds often change from northern winds
24 to southern ones during noontime (Lin et al., 2009; Lin et al., 2012). SO₂ noontime peak cases
25 with the above described change in wind direction and with maximum wind speeds below 7 m s⁻¹
26 were counted into the mountain valley breezes case (Chen, 2009).

27 Severe haze or fog events are characterized by high RH values. For SDZ, GCH and WQ, the
28 fog or severe haze event is defined as a case with RH exceeding 90% for over 5 consecutive
29 hours. Since CMA is located in urban Beijing and the site is surrounded by heat sources, RH
30 measured at CMA seldom reaches 90%. If the RHs at CMA exceed 80% for over 5 consecutive

1 hours and the other 3 stations simultaneously show RH greater than 90%, then it is believed
2 that CMA is also experiencing a fog or severe haze event.

3 **2.4 Evaluation of the impacts of the SO₂ noon peak phenomenon on the** 4 **sulphur cycle**

5 To analyse how the SO₂ diurnal variation pattern influences the sulphur cycle, the WQ site of
6 the HaChi Campaign has been selected to represent the polluted background of the NCP.
7 Normalized SO₂ diurnal variation patterns, which were already grouped based on Sect. 2.2,
8 were averaged respectively for summer (Jul to Aug), autumn (Sep to Nov) and winter (Dec to
9 Jan). The occurrence frequency of each group in each season is calculated. The average SO₂
10 daily maximum value of each season, which is 20, 40 and 75 ppbv for summer, autumn and
11 winter, respectively, is multiplied with the average normalized diurnal patterns to yield
12 characteristic SO₂ diurnal concentration variation patterns for the three groups and for each
13 season.

14 The characteristic SO₂ diurnal concentration variation patterns of the three groups will yield
15 different dry deposition, gas phase oxidation and aqueous phase transformation amounts, which
16 will be compared against each other. The occurrence frequency of the three groups will also be
17 considered to show how the actual diurnal variation pattern influences the sulphur cycle.

18 **2.4.1 The impact on dry deposition**

19 The dry deposition velocity of SO₂ is influenced by the surface type, roughness and the near
20 surface turbulent mixing strength. Surfaces covered by vegetation usually show high SO₂ dry
21 deposition rates during noontime and lower ones during nighttime due to transpiration
22 processes and the strong noontime turbulent mixing processes (Tsai et al., 2010; Raymond et
23 al., 2004). SO₂ concentration peaking during noontime instead of nighttime would increase SO₂
24 dry deposition fluxes, leading to increased acid depositions.

25 To study the impact of the SO₂ diurnal variation pattern on dry deposition fluxes, the diurnal
26 variation of the dry deposition velocity v_d measured by Tsai et al. (2010) is used and the dry
27 deposition flux is calculated by:

$$28 \quad F = C \cdot v_d, \quad (1)$$

29 where C is the SO₂ concentration, which will be provided by the characteristic SO₂ diurnal
30 concentration variation pattern. The dry deposition velocity in the NCP is ranges from 0.2 to

1 0.8 cm s⁻¹, showing no significant seasonal variations (Pan et al., 2013), which conforms well
2 with the result of Tsai et al. (2010). Thus, it is believed to be appropriate to use the diurnal
3 pattern measured by Tsai et al. (2010) for the NCP region. The total daily dry deposition flux
4 of group 2 and group 3 is compared against that of group 1. The daily dry deposition flux of the
5 three groups are averaged weighted by the occurrence frequency of those three groups and is
6 also compared against that of group 1. This will show how the SO₂ diurnal variation
7 characteristics in the NCP increase the dry depositions compared to the common nighttime peak
8 pattern observed in other places of the world.

9 2.4.2 The impact on gaseous oxidation

10 The NCAR Master Mechanism (NCAR-MM version 2.4) photochemical box model is used to
11 calculate the homogeneous diurnal oxidation process of SO₂ (Madronich, 2006; Madronich and
12 Calvert, 1990). The model is coupled with a Tropospheric Ultraviolet and Visible Radiation
13 (TUV) model (Madronich and Flocke, 1999), which calculates the photolysis rates needed for
14 photolytic reactions. The radiative properties of the 1st Jul 2009, 1st Oct 2009 and 1st Jan 2010
15 were modelled to represent the summer, autumn and winter cases, respectively.

16 Detailed oxidation processes of SO₂ with various atmospheric oxidants (e.g. OH, O₃, NO_x and
17 organic radicals) are included in the model. The concentration of O₃ and NO_x are constrained
18 according to the seasonally averaged diurnal profiles measured during the Hachi Summer
19 Campaign, while that of VOCs could only be constrained according to summertime
20 measurements (Ran et al., 2011). To evaluate the sensitivity of the modelling results to the
21 VOCs concentration assumptions, two additional case scenarios with doubled the amount of
22 summer time VOCs accompanied by half the amount of isoprene and with tripled the amount
23 of summer time VOCs accompanied by a third of the amount of isoprene were calculated. SO₂
24 concentrations are constrained by the characteristic diurnal variation patterns of the three groups
25 for the three seasons. The entrainment, dilution and dilution processes have been turned off to
26 focus on the oxidation process.

27 The daily gas phase oxidized SO₂ amount of group 2 and group 3 is compared against that of
28 group 1. The daily gas phase oxidized SO₂ amount of the three groups are averaged weighted
29 by the occurrence frequency of those three groups and is also compared against that of group 1.

30

1 2.4.3 The impact on aqueous oxidation

2 The SO₂ aqueous oxidation process depends on the atmospheric liquid water content (LWC) as
3 well as the concentration of atmospheric oxidants. For the aqueous phase oxidation of SO₂ the
4 most important two oxidants are H₂O₂ and O₃ (Seinfeld and Pandis, 2006).

5 The aqueous phase oxidized SO₂ amount can be estimated with the following two equations:

$$6 \Delta S(\text{IV}) = (k_1 [\text{SO}_2 \cdot \text{H}_2\text{O}] + k_2 [\text{HSO}_3^-] + k_3 [\text{SO}_3^{2-}]) \cdot [\text{O}_3] \cdot \Delta t \cdot \text{LWC} \cdot 10^{-6}, \quad (2)$$

$$7 \Delta S(\text{IV}) = \frac{k_4 [\text{H}^+][\text{HSO}_3^-]}{1+k_5 [\text{H}^+]} \cdot [\text{H}_2\text{O}_2] \cdot \Delta t \cdot \text{LWC} \cdot 10^{-6}, \quad (3)$$

8 where k_1, \dots, k_5 are $2.4 \times 10^4 \text{ mol}^{-1} \text{ s}^{-1}$, $3.7 \times 10^5 \text{ mol}^{-1} \text{ s}^{-1}$, $3.7 \times 10^5 \text{ mol}^{-1} \text{ s}^{-1}$, $1.5 \times 10^9 \text{ mol}^{-1} \text{ s}^{-1}$,
9 $7.5 \times 10^7 \text{ mol}^{-2} \text{ s}^{-1}$, 13 mol^{-1} , respectively (Seinfeld and Pandis, 2006). The dissolved
10 concentrations of SO₂, O₃ and H₂O₂ can be calculated with the Henry's Law.

11 Atmospheric LWC exists mostly in clouds, which makes the diurnal variation of atmospheric
12 LWC very complicated. For this study, LWC is assumed to be a constant value 0.029 g m^{-3}
13 throughout the day based on the aircraft measurements of clouds over the NCP (Deng et al.,
14 2009). The pH value is fixed to 5.5 (Sun et al., 2010). The diurnal variation O₃ concentration
15 pattern is set according to Sect. 2.4.2. The H₂O₂ diurnal variation pattern shape is adopted from
16 Hua et al. (2008), due to their relatively long measurement period. The daily maximum H₂O₂
17 value during summer is set according to measurements in Beijing (He et al., 2010), while those
18 in autumn and winter are set to 0.9 and 0.3 based on the H₂O₂ concentration ratio of
19 autumn/winter to summer in (Sakugawa et al., 1990). The SO₂ concentration pattern is set
20 according to the characteristic diurnal variation patterns of the three groups for the three seasons.
21 The daily aqueous phase oxidized SO₂ amount of group 2 and group 3 is compared against that
22 of group 1. The occurrence frequency weighting averaged results of the three groups is also
23 compared against that of group 1.

24 It should be noted that, certain uncertainties will be introduced into this estimation by assuming
25 that trace gas concentrations at cloud level are the same as at ground level. However, the
26 uncertainty will be only shown in the absolute aqueous oxidized amount and will not have
27 influences on the inter-comparison between the groups.

28

1 **3 Results and Discussions**

2 **3.1 SO₂ noontime peak phenomenon in the NCP**

3 While the SO₂ diurnal variation in other parts of the world were typically characterized by
4 higher values during the night and lower ones during the day, this NCP study has revealed a
5 time reversal of SO₂ variation characteristics.

6
7 Figure 2a-d displays the season-diurnal variation of SO₂ concentrations at SDZ, CMA, GCH
8 and WQ, respectively. It can be noted that SO₂ concentrations are usually higher in cold seasons,
9 due to enhanced emissions, weakened removal processes and lower PBLH. Significantly
10 elevated SO₂ values during noontime throughout all the seasons were found at the GCH and
11 WQ stations (Figure 2c and d). At SDZ, high SO₂ concentrations occur during noontime in all
12 seasons, except for the winter season (Figure 2a). At CMA, noontime SO₂ peaks could only be
13 observed in spring and autumn, while in winter high SO₂ concentrations occur both during early
14 noon and nighttime (Figure 2b).

15
16 The SO₂ noontime peak seems to be a common phenomenon throughout the NCP region,
17 especially at the WQ and GCH site, at which the measurements are more representative of the
18 regional background pollution. However, how frequently such events occur, what the causes
19 are and what impacts they may have on atmospheric chemistry, cloud physics and climate is
20 still unknown.

21
22 For the study of the average diurnal pattern, normalized diurnal patterns were calculated and
23 classified into the Nighttime-Peak group (group 1), the Noontime-Peak group (group 2) and the
24 Nighttime & Noontime group (group 3). The average normalized diurnal variation pattern of
25 each group, the according SEM and the occurrence frequency of each group is displayed in
26 Figure 3.

27
28 As depicted in Figure 3a1-d1, the total SO₂ noontime peak occurrence frequency (group 2 +
29 group 3) respectively reached 58%, 50%, 72% and 69% at the SDZ, CMA, GCH and WQ
30 station. Days with only one noontime peak were more common (SDZ: 43%, CMA: 31%, GCH:
31 47%, WQ: 44%), while cases with both noontime and nighttime peaks also often occurred (SDZ:
32 15%, CMA: 19%, GCH: 25%, WQ: 25%). At SDZ, GCH and WQ, the average normalized SO₂

1 concentration reaches its peak at 12 am, while at CMA the peak occurs between 10 to 11 am.
2 The averaged diurnal variation pattern of group 3 shows lower peak values than group 2 and
3 the peaks tend to occur 1 hour earlier than in group 2. However, both group 2 and group 3 for
4 SO₂ reveal distinct noontime peaks.

5
6 The averaged diurnal patterns of CO for the CMA, GCH and WQ sites resemble each other in
7 shape. The normalized CO concentrations of group 2 and group 3 all show peaks at 9 am, which
8 can also be seen as late morning peaks. At SDZ, the CO peak of group 2 occurs between 12 am
9 to 2 pm, while that of group 3 is also found between 9 to 10 am. The total noontime peak
10 occurrence frequency of CO for SDZ, CMA, GCH and WQ is 30%, 39%, 40% and 55%,
11 respectively.

12
13 The total occurrence frequencies of noontime SO₂ peaks in each month for the four stations are
14 listed in Table 1. Distinctly higher occurrence frequencies during warmer seasons were found
15 in SDZ, while in CMA the occurrence frequencies are high in spring and autumn. Noontime
16 peak occurrence frequencies in GCH show less regular seasonal variations, while those in WQ
17 are relatively lower in summer and higher in autumn and winter.

18
19 It can be concluded that, the SO₂ noontime peak phenomenon occurs frequently at the NCP
20 sites, regardless of seasons. The average peak is mostly reached at 12 am. The highest noontime
21 peak occurrence frequencies were found at GCH and WQ, the two sites that are most
22 representative of the background pollution state of the NCP. Only a few CO noontime peaks
23 were found and most of them are late morning peaks.

24

25 **3.2 Causes for SO₂ noontime peak phenomenon**

26 Different from the SO₂ diurnal patterns in other places of the world, the high SO₂ emissions
27 and concentrations together with the special topography and meteorological characteristics in
28 the NCP have led to a unique noontime peak pattern. The SO₂ noontime peak could be attributed
29 to four possible causes.

30

31 PBL mixing is strongest during noontime, during which down-mixing processes of elevated
32 SO₂ polluted layers will be enhanced. Elevated SO₂ pollution layers could have formed through

1 the emission of stacks whose plumes can rise above the surface temperature inversion layer or
2 through the mountain-chimney-effect (Chen et al., 2009), in which surface SO₂ plumes are
3 inject into the free troposphere through valley winds during the afternoon and transported back
4 to the plain with westerly winds. As is shown in Figure 4, temperature inversions during 08 LT
5 are most common in autumn and winter, with occurrence frequencies exceeding 80% of the
6 days. In spring and summer, over 60% of the days experienced temperature inversions at 08 LT.
7 Inversion depth are typically shallow, with 89%, 98%, 72% and 73% of the days showing
8 inversion layers depths less than 250 m during spring, summer, autumn and winter 2009,
9 respectively. Inversion depth are especially shallow in spring and summer, with over 80 and
10 96% of the days showing inversion layers below 100 m, respectively. Stacks of industries and
11 power plants are typically 10 to 240 m high and the higher stacks are emitting a significantly
12 larger amount of SO₂ compared to the smaller stacks (Wang et al., 2006a; Yang et al., 2008; Zhou
13 et al., 2003). Additionally, due to the plume rise process, the effective plume height could be
14 much higher than the stack heights (Slawson and Csanady, 1971). Thus, the frequent occurrence
15 of shallow inversions together with the large amount of SO₂ that is released from higher stacks
16 will favor the formation of elevated SO₂ pollution layers. The average normalized SO₂, CO and
17 temperature profiles that were filed under the down-mixing case category are displayed in
18 Figure 5a1-a4. Down-mixing case samples take up 34%, 30%, 43% and 52% of the noontime
19 peaks at SDZ, CMA, GCH and WQ, respectively (Table 2a).

20
21 The transport of SO₂ plumes can result in sudden increases of local SO₂ concentrations. The
22 plume transport process is characterized by the coherent variation of SO₂ and CO. The average
23 normalized SO₂, CO and temperature profiles in the plume transport case can be seen in Figure
24 5b1-b4. Although SO₂ shows a peak between 9 and 12 am, the occurrence time of the peaks
25 caused by plume transport processes was rather random. This process respectively explains
26 21%, 46%, 20% and 30% of the noontime peaks at SDZ, CMA, GCH and WQ (Table 2b). It
27 should be noted that, due to our classification method, cases with SO₂ and CO both having a
28 late morning peak are also included into this category.

29
30 Mountain valley circulations lead to diurnal variations in wind directions, thus resulting in a
31 diurnal variation in pollutant transport. Due to the topography of the NCP, all four sites are
32 under the influence of mountain valley circulations, especially the SDZ, CMA and GCH sites.
33 Winds often change from northern winds to southern ones during noontime. Due to the stronger

1 SO₂ emissions and resulting higher concentrations in the southern part of the NCP (Figure 1),
2 southern winds will aid the transport of polluted air masses to our stations. The average diurnal
3 patterns in the mountain valley breezes case are shown in Figure 5a3-d3. A change in wind
4 direction takes place between 8 am to 12 am, while SO₂ starts increasing before noon and
5 reaches its peak between 12 am and 4 pm at all four stations. As can be seen in Table 2c, the
6 mountain valley breeze factor can respectively explain 40%, 20%, 20% and 6% of the noontime
7 peaks occurring in SDZ, CMA, GCH and WQ. Since SDZ is a relatively clean background site,
8 the mountain-valley breeze will not only cause increasing noontime SO₂ concentrations but also
9 increasing CO concentrations. This explains why only the SDZ site showed noontime CO peaks
10 in Figure 3.

11
12 Aerosol and fog liquid water can serve as an efficient sink for SO₂. SO₂ is a soluble gas, which
13 can be scavenged effectively through aqueous phase reactions in fog or wet aerosol particles
14 (Pandis et al., 1992). Fog and high RH haze events usually occur during nighttime and persist
15 until the temperature rises up in the morning, leading to low nighttime SO₂ concentrations.
16 Additionally, such events are typically characterized by surface temperature inversions, which
17 will prevent the down-mixing of elevated SO₂ emissions (Jacobson, 2002). With the increasing
18 temperature in the morning, the RH will decrease, weakening the SO₂ scavenging process. The
19 temperature inversion will vanish, allowing for the down-mixing of SO₂ from aloft. Averaged
20 normalized SO₂, CO and RH profiles in the fog or severe haze case are shown in Figure 5d1-
21 d4. SO₂ peaks were reached typically between 12 am and 16 pm, depending on how long the
22 fog or high RH event lasted. Such events caused 5%, 4%, 18% and 12% of the noontime peak
23 events at SDZ, CMA, GCH and WQ, respectively.

24

25 **3.3 Impacts of SO₂ noontime peak phenomenon on the sulphur cycle**

26 SO₂ peaks occurring during noontime instead of nighttime might have remarkable impacts on
27 human health, environment and climate. Higher SO₂ concentrations during daytime will not
28 only pose higher health risks for humans, but also change the sulphur cycle.

29 For surfaces covered with vegetation, dry deposition processes are typically most dynamic
30 during noontime due to transpiration processes and the strong turbulent mixing processes
31 (Raymond et al., 2004; Tsai et al., 2010), thus noontime SO₂ peaks may create more acid

1 deposition than common nighttime peak variation patterns. The calculated diurnal dry
2 deposition fluxes based on the diurnal dry deposition velocity in Tsai et al. (2010) and the
3 characteristic SO₂ diurnal variations of the three groups in WQ during autumn are shown in
4 Figure 6. Group 2 and 3 show significantly higher dry deposition fluxes than group 1 during 8
5 am to 6 pm (LT), while for the other time periods the dry deposition fluxes of the three groups
6 are similar to one another. The estimated daily deposition fluxes for summer, winter and autumn
7 in WQ are listed in Table 3. Seasonally, dry deposition fluxes are higher during colder seasons
8 than during warmer ones, due to elevated SO₂ concentrations and due to the fact that seasonal
9 variations in dry deposition rates were not considered. Within the same season, the occurrence
10 time of the SO₂ peak had major impacts on the daily dry deposition fluxes. The results of group
11 2 show a 22 to 46% increase in daily dry deposition flux compared to those of group 1, while
12 those of group 3 show a 44 to 62% increase. Considering the occurrence frequency of the three
13 diurnal patterns, the weighting averaged daily dry deposition fluxes show increases of 13 to 35%
14 relative to the common nighttime peak case, with the lowest increase occurring during summer
15 and the highest one during autumn.

16 Atmospheric photochemistry is most active during noontime due to favourable radiative
17 conditions. The simulated SO₂ gas phase conversion processes for the three SO₂ diurnal
18 variation patterns in WQ during autumn are displayed in Figure 7. Due to the fact that
19 deposition processes have been turned off in the simulations, S(VI) products will accumulate
20 in the air parcel. Accumulated S(VI) concentrations of group 3 are the highest throughout the
21 day, while that of group 2 exceeds that of group 1 after 10 am. The SO₂ oxidation rates of group
22 2 and 3 during noontime are significantly higher than those of group 1. The simulated daily gas
23 phase SO₂ conversion amount for summer, winter and autumn in WQ are listed in Table 4.
24 Despite the weakened photochemistry during winter, the high SO₂ concentration in winter has
25 led to higher gas phase oxidized SO₂ amounts than in summer. SO₂ noontime peak patterns
26 could also increase the daily gas phase oxidized SO₂ amount. The results of group 2 show a 15
27 to 26% increase in gas phase oxidized amount compared to those of group 1, while those of
28 group 3 show a 28 to 50% increase. Considering the occurrence frequency of the three diurnal
29 patterns, the weighting averaged gas phase oxidized amounts show increases of 9 to 23%
30 relative to the common nighttime peak case, with the lowest increase occurring during summer
31 and the highest one in winter. Increased VOCs concentrations during autumn and winter will
32 lead to increased SO₂ oxidized amounts, however, the relative increase of group 2 and group 3

1 to that of group 1 decreases slightly with increasing VOCs concentrations. Overall, the VOCs
2 concentrations have little influence in the inter-comparison between the three groups.

3 Concentrations of atmospheric oxidants that are important in SO₂ aqueous phase reactions also
4 reach their peaks during noontime. Assuming a constant LWC throughout the day and assuming
5 that concentrations near clouds are similar to the surface concentrations, the estimated SO₂
6 aqueous phase conversion rate for the three SO₂ diurnal variation patterns in WQ during autumn
7 are displayed Figure 8. SO₂ conversion amounts of group 2 and 3 are significantly higher than
8 those of group 1 during 8 am to 6 pm, with that of group 2 being highest between 11 am to 4
9 pm. The simulated daily aqueous phase SO₂ conversion amount for summer, winter and autumn
10 in WQ are listed in Table 5. The aqueous phase scavenged SO₂ amounts during the three
11 seasons are on the same level. The high SO₂ concentrations in winter have been cancelled out
12 by the low concentrations in oxidants. The diurnal variation pattern however had much impact
13 on the aqueous phase oxidized SO₂ amount. Compared to group 1, group 2 shows a 13 to 43%
14 increase in aqueous phase conversion amount, while group 3 shows a 28 to 61% increase.
15 Considering the occurrence frequency of the three diurnal patterns, the weighting averaged
16 aqueous phase SO₂ conversion amounts show increases of 8 to 33% relative to the common
17 nighttime peak case, with the lowest increase occurring during summer and the highest one
18 during autumn.

19 In all, compared to the nighttime SO₂ peak case, which was observed all around the world, the
20 NCP experienced enhanced sulphur dry depositions and sulphur to sulphate conversions due to
21 the frequently occurring SO₂ noontime peak phenomenon. More acidic deposition is formed.
22 Aerosols in the NCP will show higher sulphate fractions and become more hygroscopic (Liu et
23 al., 2013). This will promote the light scattering effect of aerosols and thus may have important
24 impacts on regional climate.

25

26 **4 Summary**

27 In this paper, a frequently occurring SO₂ noontime peak pattern was found in the NCP. A
28 detailed analysis of this SO₂ diurnal pattern, the causes for such a phenomenon and the potential
29 impacts of the phenomenon on the sulphur cycle were investigated.

30 The total noontime peak occurrence frequency reaches 68%, 50%, 72% and 69% in SDZ, CMA,
31 GCH and WQ, respectively. Down-mixing of elevated pollution layers, plume transport
32 processes, mountain-valley-winds and fog/high RH haze events were the possible causes. The

1 contribution of each process varies from each other and from station to station, which the down-
2 mixing process being the most important process at three out of four stations. However, none
3 of those four processes is negligible. The different occurrence frequencies of noontime peak
4 phenomenon and the different contribution of each process to each site has led to distinct
5 noontime peak occurrence times in the long-term averaged diurnal profiles at the different types
6 of sites.

7 The SO₂ noontime peak phenomenon significantly speeds up the sulphur cycle. Compared to
8 the nighttime SO₂ peak case, which was observed all around the world, WQ respectively
9 experienced 13 to 35%, 9 to 23% and 8 to 33% enhancement in sulphur dry depositions, gas
10 phase oxidations and aqueous phase conversions due to the frequently occurring SO₂ noontime
11 peak phenomenon.

12 SO₂ peaks occurring during noontime instead of nighttime has led to more acidic deposition.
13 Aerosols in the NCP will show higher sulphate fractions and become more hygroscopic. This
14 will promote the light scattering effect of aerosols and thus may have important impacts on
15 regional climate. Higher SO₂ concentrations during daytime will also pose higher health risks
16 for human. The potential impacts of such a phenomenon on human health, environment and
17 climate should be studied in detail in the future.

18

19 **Acknowledgements**

20 This work is supported by the National 973 project of China (2011CB403402), National Natural
21 Science Foundation of China (41375134), Beijing Natural Science Foundation (8131003) and
22 the Basic Research Fund of Chinese Academy of Meteorological Sciences (2011Z003).

- 1 Lin, W., Xu, X., Zhang, X., and Tang, J.: Contributions of pollutants from North China Plain
2 to surface ozone at the Shangdianzi GAW Station, *Atmos. Chem. Phys.*, 8, 5889-5898,
3 10.5194/acp-8-5889-2008, 2008.
- 4 Lin, W., Xu, X., Ge, B., and Zhang, X.: Characteristics of gaseous pollutants at Gucheng, a
5 rural site southwest of Beijing, *J. Geophys. Res.*, 114, D00G14, 10.1029/2008jd010339, 2009.
- 6 Lin, W., Xu, X., Ge, B., and Liu, X.: Gaseous pollutants in Beijing urban area during the heating
7 period 2007–2008: variability, sources, meteorological, and chemical impacts, *Atmos. Chem.*
8 *Phys.*, 11, 8157-8170, 10.5194/acp-11-8157-2011, 2011.
- 9 Lin, W., Xu, X., Ma, Z., Zhao, H., Liu, X., and Wang, Y.: Characteristics and recent trends of
10 sulfur dioxide at urban, rural, and background sites in North China: Effectiveness of control
11 measures, *Journal of Environmental Sciences*, 24, 34-49, [http://dx.doi.org/10.1016/S1001-](http://dx.doi.org/10.1016/S1001-0742(11)60727-4)
12 [0742\(11\)60727-4](http://dx.doi.org/10.1016/S1001-0742(11)60727-4), 2012.
- 13 Liu, H. J., Zhao, C. S., Nekat, B., Ma, N., Wiedensohler, A., van Pinxteren, D., Spindler, G.,
14 Müller, K., and Herrmann, H.: Aerosol hygroscopicity derived from size-segregated chemical
15 composition and its parameterization in the North China Plain, *Atmos. Chem. Phys. Discuss.*,
16 13, 20885-20922, 10.5194/acpd-13-20885-2013, 2013.
- 17 Liu, P. F., Zhao, C. S., Göbel, T., Hallbauer, E., Nowak, A., Ran, L., Xu, W. Y., Deng, Z. Z.,
18 Ma, N., Mildenberger, K., Henning, S., Stratmann, F., and Wiedensohler, A.: Hygroscopic
19 properties of aerosol particles at high relative humidity and their diurnal variations in the North
20 China Plain, *Atmos. Chem. Phys.*, 11, 3479-3494, 10.5194/acp-11-3479-2011, 2011.
- 21 Madronich, S., and Calvert, J. G.: Permutation reactions of organic peroxy radicals in the
22 troposphere, *Journal of Geophysical Research: Atmospheres*, 95, 5697-5715,
23 10.1029/JD095iD05p05697, 1990.
- 24 Madronich, S., and Flocke, S.: The role of solar radiation in atmospheric chemistry, in: *The*
25 *Handbook of Environmental Chemistry*, edited by: Boule, P., Springer-Verlag Berlin
26 Heidelberg, 1-26, 1999.
- 27 Madronich, S.: Chemical evolution of gaseous air pollutants down-wind of tropical megacities:
28 Mexico City case study, *Atmospheric Environment*, 40, 6012-6018,
29 <http://dx.doi.org/10.1016/j.atmosenv.2005.08.047>, 2006.
- 30 Pan, Y. P., Wang, Y. S., Tang, G. Q., and Wu, D.: Spatial distribution and temporal variations
31 of atmospheric sulfur deposition in Northern China: insights into the potential acidification
32 risks, *Atmos. Chem. Phys.*, 13, 1675-1688, 10.5194/acp-13-1675-2013, 2013.
- 33 Pandis, S. N., Seinfeld, J. H., and Pilinis, C.: Heterogeneous sulfate production in an urban fog,
34 *Atmospheric Environment. Part A. General Topics*, 26, 2509-2522,
35 [http://dx.doi.org/10.1016/0960-1686\(92\)90103-R](http://dx.doi.org/10.1016/0960-1686(92)90103-R), 1992.
- 36 Psiloglou, B., Larissi, I., Petrakis, M., Paliatsos, A., Antoniou, A., and Viras, L.: Case studies
37 on summertime measurements of O₃, NO₂, and SO₂ with a DOAS system in an urban semi-
38 industrial region in Athens, Greece, *Environmental Monitoring and Assessment*, 185, 7763-
39 7774, 10.1007/s10661-013-3134-2, 2013.
- 40 Qi, H., Lin, W., Xu, X., Yu, X., and Ma, Q.: Significant downward trend of SO₂ observed from
41 2005 to 2010 at a background station in the Yangtze Delta region, China, *Science China*
42 *Chemistry*, 55, 1451-1458, 10.1007/s11426-012-4524-y, 2012.
- 43 Ran, L., Zhao, C. S., Xu, W. Y., Lu, X. Q., Han, M., Lin, W. L., Yan, P., Xu, X. B., Deng, Z.
44 Z., Ma, N., Liu, P. F., Yu, J., Liang, W. D., and Chen, L. L.: VOC reactivity and its effect on

1 ozone production during the HaChi summer campaign, *Atmos. Chem. Phys.*, 11, 4657-4667,
2 10.5194/acp-11-4657-2011, 2011.

3 Raymond, H. A., Yi, S.-M., Moumen, N., Han, Y., and Holsen, T. M.: Quantifying the dry
4 deposition of reactive nitrogen and sulfur containing species in remote areas using a surrogate
5 surface analysis approach, *Atmospheric Environment*, 38, 2687-2697,
6 <http://dx.doi.org/10.1016/j.atmosenv.2004.02.011>, 2004.

7 Sakugawa, H., Tsai, W., Kaplan, I. R., and Cohen, Y.: Factors controlling the photochemical
8 generation of gaseous H₂O₂ in the Los Angeles atmosphere, *Geophysical Research Letters*, 17,
9 93-96, 10.1029/GL017i001p00093, 1990.

10 Slawson, P., and Csanady, G.: The effect of atmospheric conditions on plume rise, *Journal of*
11 *Fluid Mechanics*, 47, 33-49, 1971.

12 Sun, M., Wang, Y., Wang, T., Fan, S., Wang, W., Li, P., Guo, J., and Li, Y.: Cloud and the
13 corresponding precipitation chemistry in south China: Water-soluble components and pollution
14 transport, *Journal of Geophysical Research: Atmospheres*, 115, D22303,
15 10.1029/2010JD014315, 2010.

16 Tsai, J.-L., Chen, C.-L., Tsuang, B.-J., Kuo, P.-H., Tseng, K.-H., Hsu, T.-F., Sheu, B.-H., Liu,
17 C.-P., and Hsueh, M.-T.: Observation of SO₂ dry deposition velocity at a high elevation flux
18 tower over an evergreen broadleaf forest in Central Taiwan, *Atmospheric Environment*, 44,
19 1011-1019, 10.1016/j.atmosenv.2009.12.022, 2010.

20 Wang, S., Hao, J., Ho, M. S., Li, J., and Lu, Y.: Intake fractions of industrial air pollutants in
21 China: Estimation and application, *Science of The Total Environment*, 354, 127-141,
22 <http://dx.doi.org/10.1016/j.scitotenv.2005.01.045>, 2006a.

23 Wang, T., Cheung, V. T. F., Lam, K. S., Kok, G. L., and Harris, J. M.: The characteristics of
24 ozone and related compounds in the boundary layer of the South China coast: temporal and
25 vertical variations during autumn season, *Atmospheric Environment*, 35, 2735-2746,
26 10.1016/s1352-2310(00)00411-8, 2001.

27 Wang, T., Cheung, T. F., Li, Y. S., Yu, X. M., and Blake, D. R.: Emission characteristics of
28 CO, NO_x, SO₂ and indications of biomass burning observed at a rural site in eastern China, *J.*
29 *Geophys. Res.*, 107, 4157, 10.1029/2001jd000724, 2002.

30 Wang, T., Wong, C. H., Cheung, T. F., Blake, D. R., Arimoto, R., Baumann, K., Tang, J., Ding,
31 G. A., Yu, X. M., Li, Y. S., Streets, D. G., and Simpson, I. J.: Relationships of trace gases and
32 aerosols and the emission characteristics at Lin'an, a rural site in eastern China, during spring
33 2001, *J. Geophys. Res.*, 109, D19S05, 10.1029/2003JD004119, 2004.

34 Wang, T., Ding, A., Gao, J., and Wu, W. S.: Strong ozone production in urban plumes from
35 Beijing, China, *Geophys. Res. Lett.*, 33, L21806, 10.1029/2006gl027689, 2006b.

36 Xu, W., Zhao, C., Ran, L., Deng, Z., Liu, P., Ma, N., Lin, W., Xu, X., and Yan, P.:
37 Characteristics of Pollutants at a Suburban Site in the North China Plain and estimated regional
38 Emissions and Contributions, *AGU Fall Meeting Abstracts*, 1, 0053, 2011a.

39 Xu, W. Y., Zhao, C. S., Ran, L., Deng, Z. Z., Liu, P. F., Ma, N., Lin, W. L., Xu, X. B., Yan, P.,
40 He, X., Yu, J., Liang, W. D., and Chen, L. L.: Characteristics of pollutants and their correlation
41 to meteorological conditions at a suburban site in the North China Plain, *Atmos. Chem. Phys.*,
42 11, 4353-4369, 10.5194/acp-11-4353-2011, 2011b.

1 Yang, D., Wang, Z., and Zhang, R.: Estimating Air Quality Impacts of Elevated Point Source
2 Emissions in Chongqing, China, *Aerosol and Air Quality Research*, 8, 279-294,
3 10.4209/aaqr.2008.02.0005, 2008.

4 Zhao, P. S., Dong, F., He, D., Zhao, X. J., Zhang, X. L., Zhang, W. Z., Yao, Q., and Liu, H. Y.:
5 Characteristics of concentrations and chemical compositions for PM_{2.5} in the region of Beijing,
6 Tianjin, and Hebei, China, *Atmos. Chem. Phys.*, 13, 4631-4644, 10.5194/acp-13-4631-2013,
7 2013.

8 Zhou, Y., Levy, J. I., Hammitt, J. K., and Evans, J. S.: Estimating population exposure to power
9 plant emissions using CALPUFF: a case study in Beijing, China, *Atmospheric Environment*,
10 37, 815-826, [http://dx.doi.org/10.1016/S1352-2310\(02\)00937-8](http://dx.doi.org/10.1016/S1352-2310(02)00937-8), 2003.

11
12
13

1 Table 1 Seasonal variation of noontime peak occurrence frequency

Month	Noontime Peak Occurrence Frequency (%)			
	SDZ	CMA	GCH	WQ
Jan	39	33	71	-
Feb	32	29	89	-
Mar	26	39	65	-
Apr	33	70	70	-
May	42	47	52	-
Jun	60	50	50	-
Jul	67	32	81	40
Aug	71	55	68	48
Sep	73	67	63	69
Oct	77	58	71	62
Nov	53	52	57	62
Dec	37	16	65	64

2

3

1 Table 2 SO₂ noontime peak occurrence frequency and the fraction of noontime peaks caused
 2 by a) down-mixing due to PBL processes, b) plume transport, c) mountain valley breezes and
 3 d) fog or severe haze events

Station	SDZ	CMA	GCH	WQ
Total Sample Count	356	374	395	180
Noontime Peak Sample Count (Occurrence Frequency)	179(50%)	165(44%)	269(68%)	105(58%)
a) Down-mixing caused Noontime Peak Sample Count	60 (34%)	50 (30%)	117 (43%)	55(52%)
b) Plume transport caused Noontime Peak Sample Count	38 (21%)	76 (46%)	53 (20%)	31(30%)
c) Mountain Valley Breeze caused Noontime Peak Sample Count	72 (40%)	33(20%)	53 (20%)	6 (6%)
d) Fog or severe haze events caused Noontime Peak Sample Count	9 (5%)	6 (4%)	49 (18%)	13 (12%)

4

5

1 Table 3 Estimated SO₂ dry deposition flux for the three different SO₂ diurnal variation patterns,
 2 the occurrence frequency (of the three groups) weighting averaged value and the relative
 3 increase compared to the nighttime peak case.

Case	SO ₂ dry deposition flux (g m ⁻² day ⁻¹)		
	[Increase relative to nighttime peak case (%)]		
	Summer	Autumn	Winter
Nighttime Peak	0.0065	0.014	0.028
Noontime Peak	0.0079 (22%)	0.020 (46%)	0.035 (27%)
Nighttime+Noontime Peak	0.0093 (44%)	0.022 (58%)	0.045 (62%)
Weighting average	0.0073 (13%)	0.019 (35%)	0.035 (28%)

4

1
2 Table 4 Simulated SO₂ gaseous oxidation amount for the three different SO₂ diurnal variation
3 patterns, the occurrence frequency (of the three groups) weighting averaged value and the
4 relative increase compared to the nighttime peak case. Case1, Case2 and Case3 respectively
5 represent cases using summertime VOCs concentrations, doubled summertime VOCs
6 concentrations with half of the summertime isoprene concentrations and tripled summertime
7 VOCs concentrations with a third of the summertime isoprene concentrations.

Case	SO ₂ gaseous oxidized amount (ppbv day ⁻¹) [Increase relative to nighttime peak case (%)]						
	summer Case1	Case1	autumn Case2	Case3	Case1	winter Case2	Case3
Nighttime	2.3	3.1	3.7	4.0	3.0	4.0	4.5
Noontime	2.6 (15%)	3.9 (26%)	4.6 (23%)	4.8 (21%)	3.7 (23%)	4.7 (18%)	5.2 (16%)
Noontime+ Nighttime	2.9 (28%)	4.3 (39%)	5.1 (36%)	5.4 (35%)	4.5 (50%)	5.9 (49%)	6.7 (49%)
Weighting Average	2.5 (9%)	3.8 (21%)	4.5 (19%)	4.7 (19%)	3.7 (23%)	4.8 (21%)	5.4 (20%)

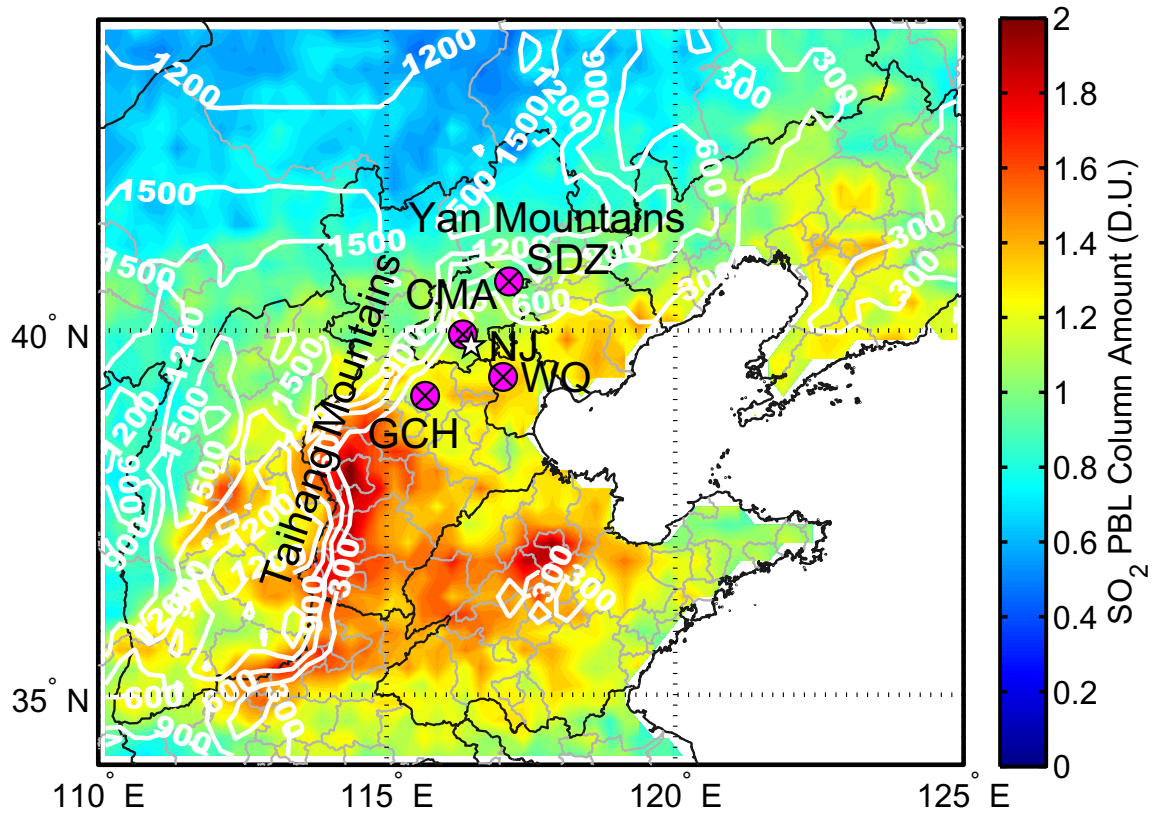
8
9

1 Table 5 Estimated SO₂ aqueous oxidation amount for the three different SO₂ diurnal variation
 2 patterns, the occurrence frequency (of the three groups) weighting averaged value and the
 3 relative increase compared to the nighttime peak case.

Case	SO ₂ aqueous oxidized amount (ppbv day ⁻¹) [Increase relative to nighttime peak case (%)]		
	Summer	Autumn	Winter
Nighttime Peak	86.5	64.2	62.4
Noontime Peak	97.5 (13%)	91.6 (43%)	77.2 (24%)
Nighttime+Noontime Peak	110.9 (28%)	99.7 (55%)	100.6 (61%)
Weighting average	93.3 (8%)	85.5 (33%)	78.8 (26%)

4

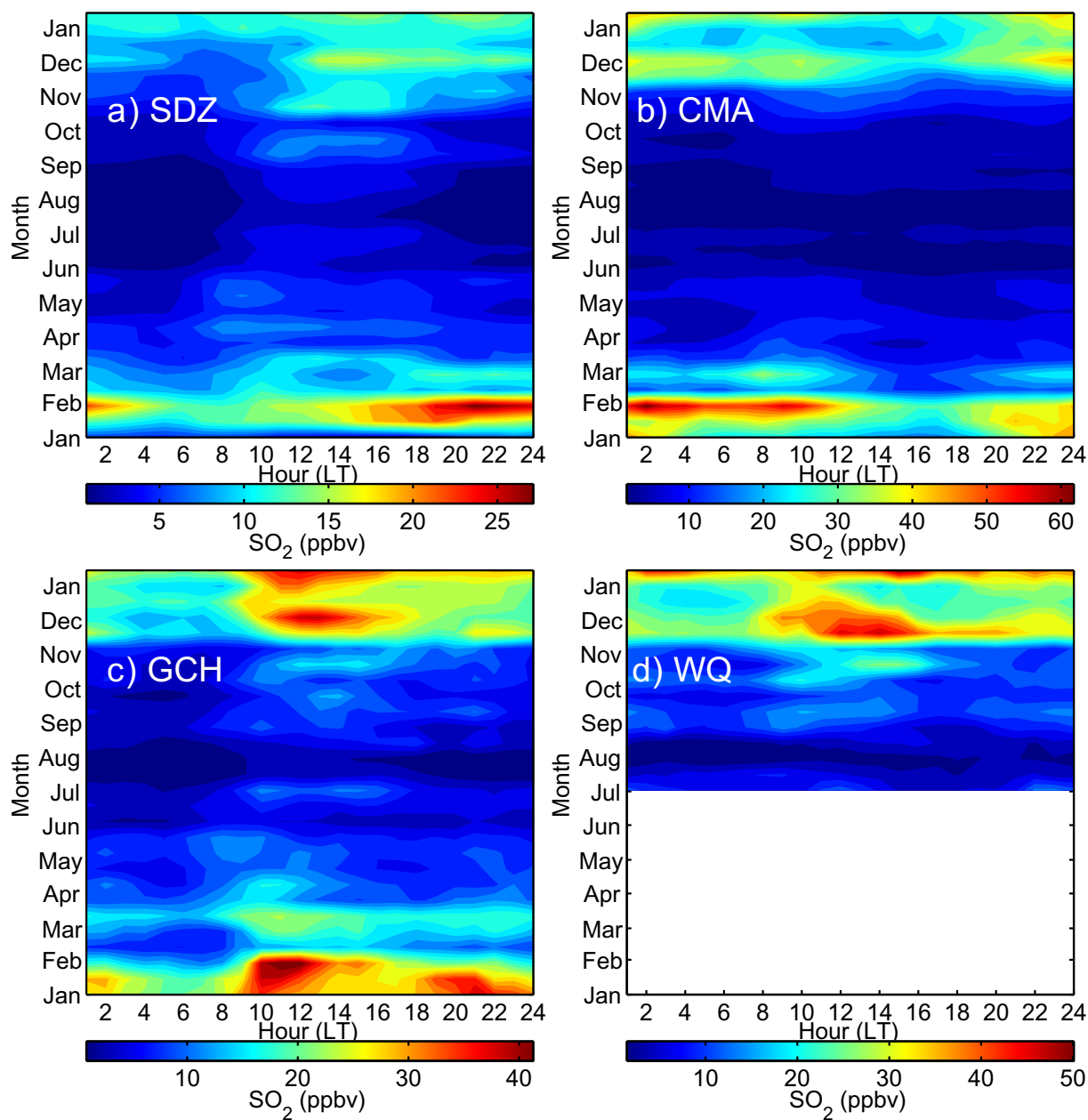
5



1

2 Figure 1 Location of the Shangdianzi (SDZ), China Meteorological Administration (CMA),
 3 Gucheng (GCH), Wuqing (WQ) site, the Nanjiao meteorological station (NJ) and the Yan and
 4 Taihang Mountains. The average distribution of OMI SO₂ column concentration in 2009 is
 5 displayed as the shaded contour, while the white contour lines show the terrain height (m).

6



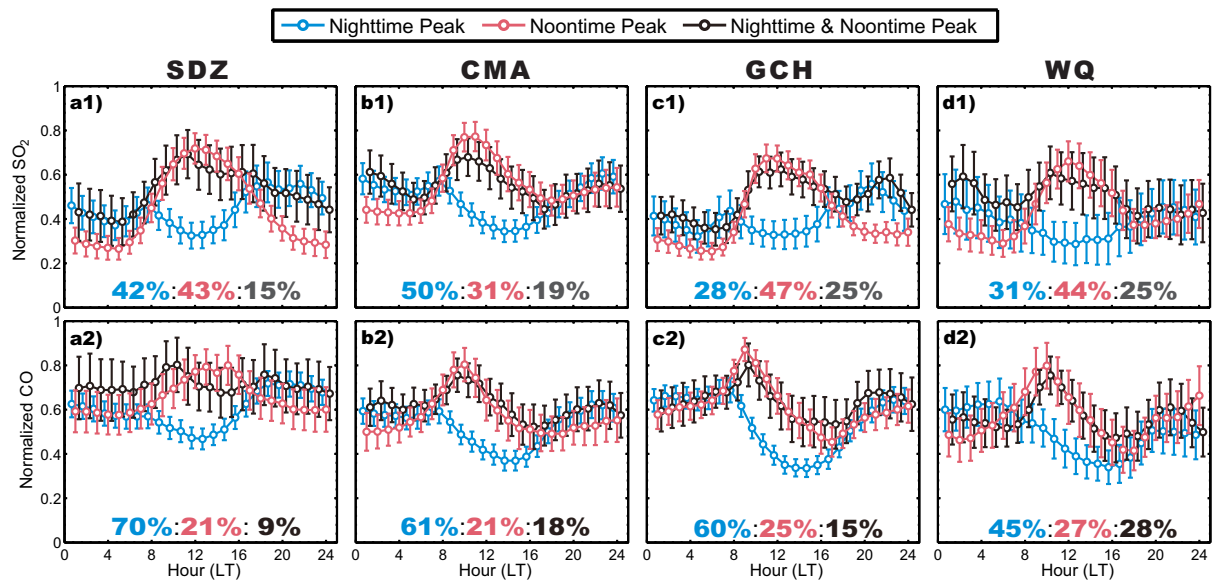
1

2 Figure 2 Diurnal and seasonal variation of SO₂ concentrations at the a) Shangdianzi, b) China

3 Meteorological Administration, c) Gucheng and d) Wuqing site.

4

5



1

2 Figure 3 Normalized 1) SO₂ and 2) CO diurnal variation pattern for the days with peaks

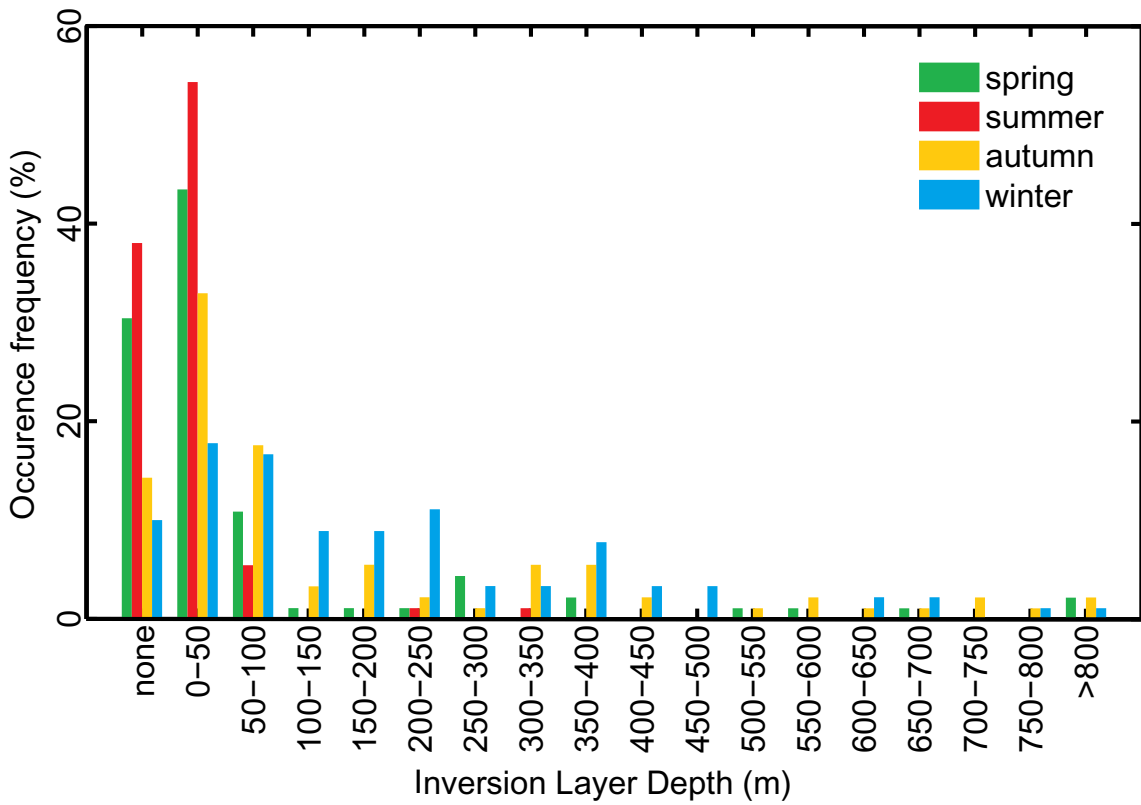
3 occurring during nighttime (blue, before 9 a.m. or after 16 p.m.), noontime (red, between 9 a.m.

4 and 16 p.m.) and during both nighttime and noontime (black) at a) Shangdianzi, b) China

5 Meteorological Administration, c) Gucheng and d) Wuqing station. The circle and error bar

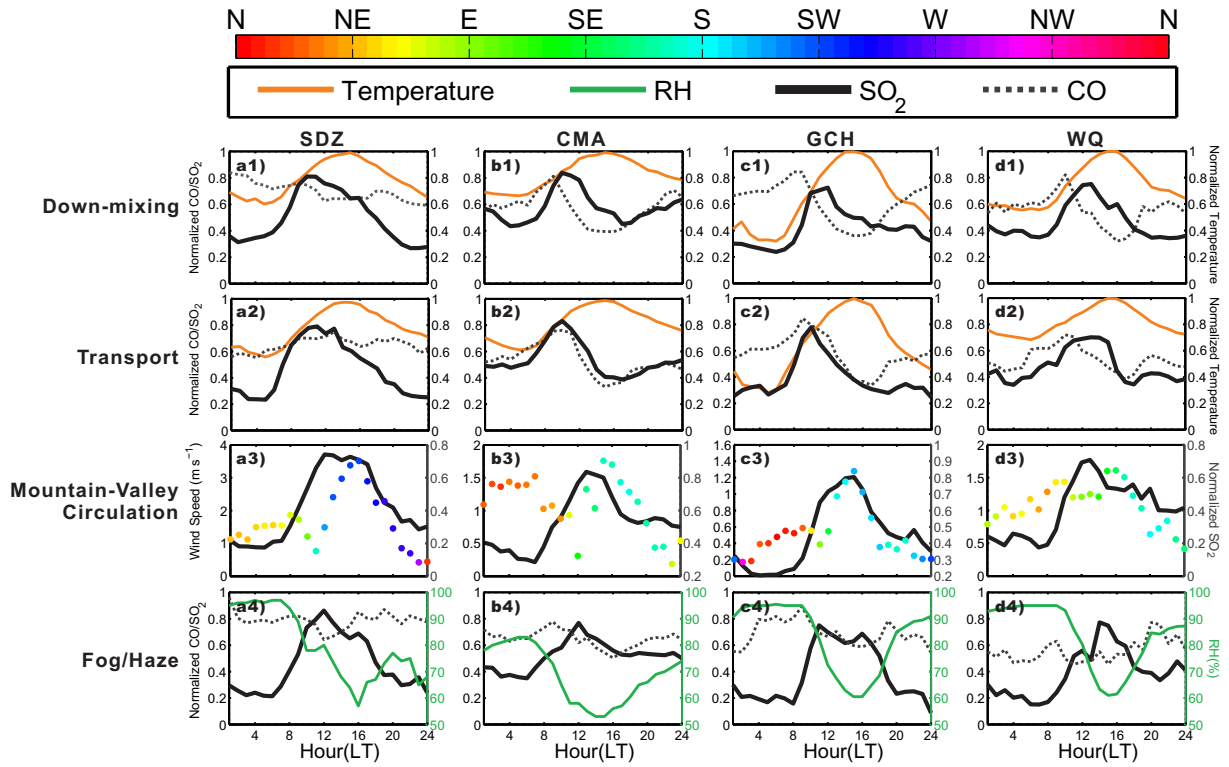
6 represent the average value \pm 3 standard error of the mean.

7



1
 2 Figure 4 The occurrence frequency of different temperature inversion layer depths during spring
 3 (Mar-May 2009), summer (Jun-Aug 2009), autumn (Sep-Nov 2009) and winter (Dec 2009 –
 4 Feb 2010) in the 08 LT radiosonde data.
 5

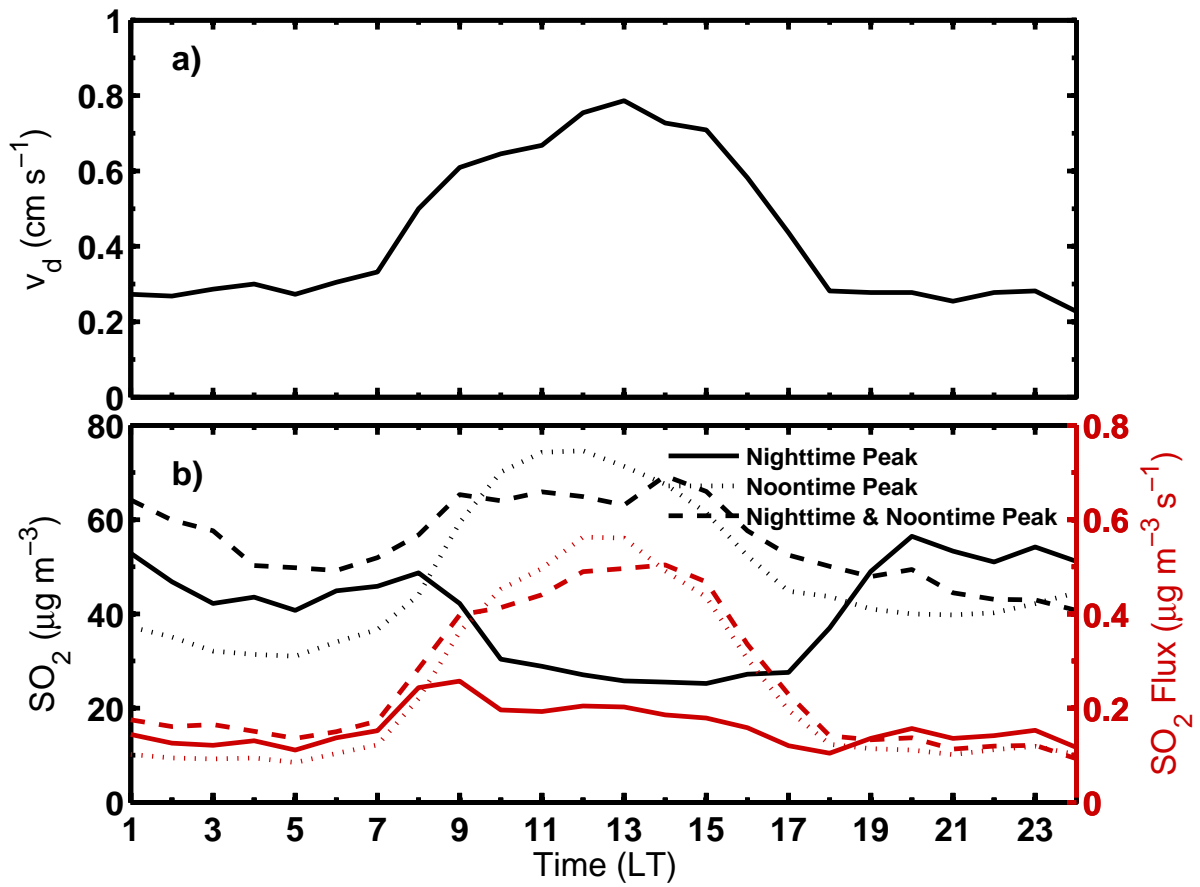
1



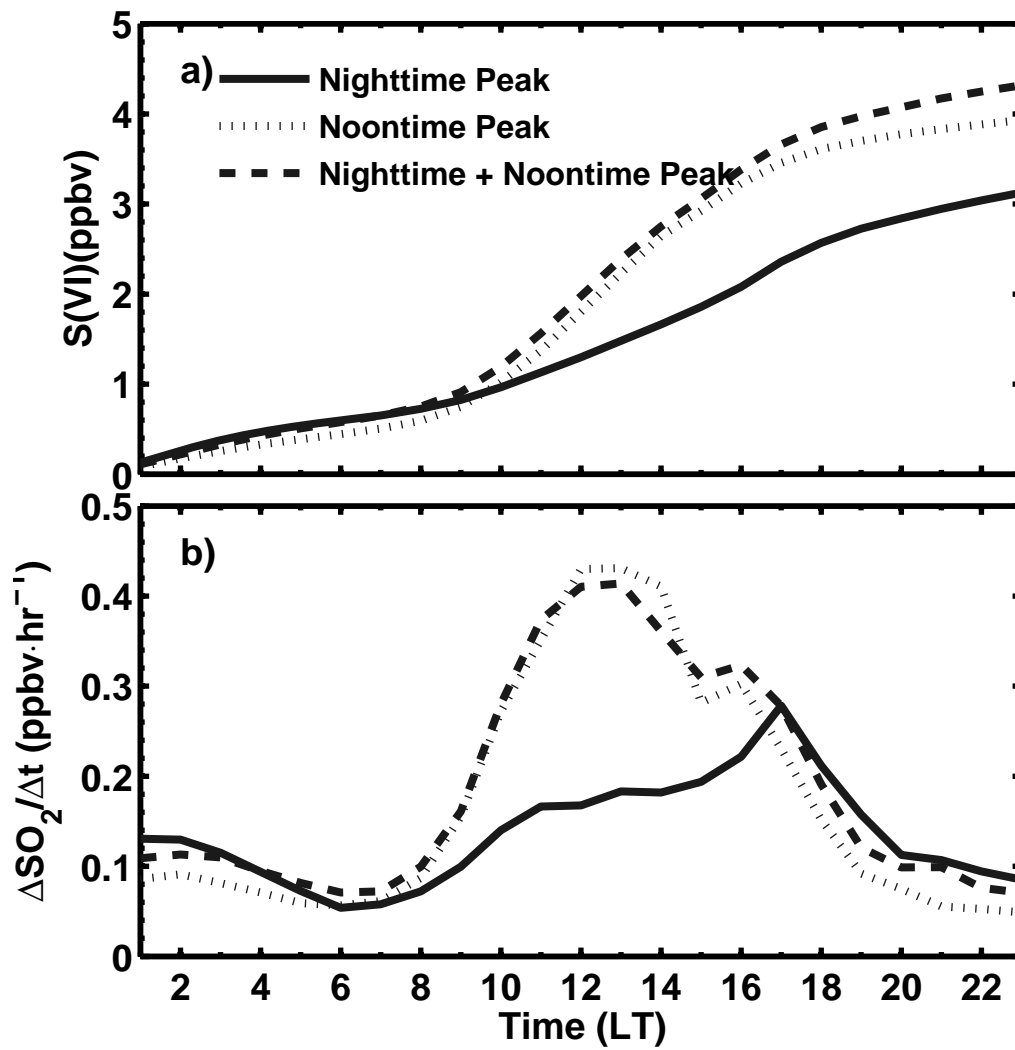
2

3 Figure 5 Averaged diurnal variation patterns for 1) the PBL down-mixing, 2) the plume
4 transport, 3) the mountain valley breeze and 4) the fog/haze case for a) Shangdianzi, b) China
5 Meteorological Administration, c) Gucheng and d) Wuqing.

6



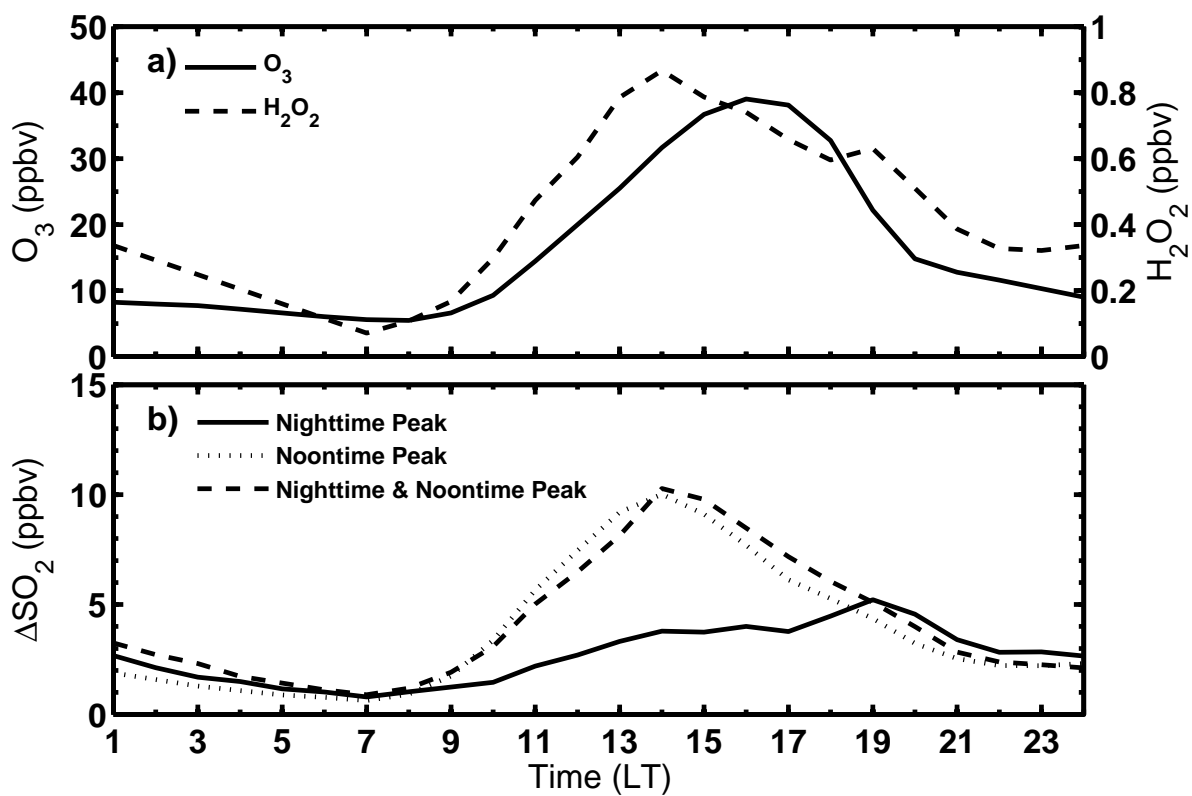
1
 2 Figure 6 a) Diurnal variation of the dry deposition velocity inferred from Tsai et al. (2010); b)
 3 Calculated dry deposition fluxes (red lines) based on the three characteristic SO_2 diurnal
 4 variation patterns (black lines) in Wuqing during autumn 2009.
 5



1

2 Figure 7 Simulated gas phase oxidized SO₂ a) amount and b) oxidation rates based on the three
 3 characteristic SO₂ diurnal variation patterns in Wuqing during autumn 2009.

4



1
 2 Figure 8 a) O_3 and H_2O_2 diurnal profiles used in the estimations; b) Estimated aqueous phase
 3 oxidized SO_2 amount based on the three characteristic SO_2 diurnal variation patterns in Wuqing
 4 during autumn 2009.
 5